



Thermal, magnetic and magnetocaloric properties of FeErNbB metallic glasses with high glass-forming ability

Feng Hu^a, Qiang Luo^a, Baolong Shen^{a,b,*}

^a School of Materials Science and Engineering, Jiangsu Key Laboratory for Advanced Metallic Materials, Southeast University, Nanjing 211189, China

^b Institute of Massive Amorphous Metal Science, China University of Mining and Technology, Xuzhou 221116, China



ARTICLE INFO

Keywords:

Fe-based BMGs
Glass-forming ability
Mechanical properties
Magnetocaloric effect

ABSTRACT

The comprehensive characteristics of Fe_{71-x}Er_xNb₆B₂₃ (x = 0, 1, 3, 5, 7 at.%) bulk metallic glasses (BMGs), including the thermal properties, glass-forming ability, magnetocaloric effect and mechanical properties were investigated. As a result, with increasing Er content up to 5 at.%, the supercooled liquid region increases to 90 K, and BMG with a critical diameter of 4 mm is fabricated by copper mold casting. The regulation of Curie temperature is achieved by controlling the amount of Er. The resulting glass alloy system exhibits Curie temperature of 340–550 K, magnetic entropy change of 0.74–1.41 J/kg K, and refrigerant capacity of 56–112 J/kg in external magnetic field of 1.5 T. Moreover, the Fe_{71-x}Er_xNb₆B₂₃ BMGs exhibit high saturation magnetic flux density of 0.43–1.09 T, high fracture strength of 3.09–4.65 GPa and high Vickers hardness of 1030–1090 kg/mm², respectively. Considering these good overall characteristics, this glass alloy system can be employed as magnetic-refrigerant materials in temperature range of 340–550 K.

1. Introduction

As a diversified alloy family, Fe-based BMGs exhibit strong potential applications owing to their excellent mechanical properties, good soft magnetic performances and low manufacturing cost [1–4]. However, the dimension of Fe-based BMGs is limited by the requirement of a high cooling rate to form the glassy alloys. Therefore, pursuing Fe-based BMGs with high glass-forming ability (GFA) has always been concerned by researchers. Recently, Fe₇₁Nb₆B₂₃ BMG was reported to exhibit a fracture strength (σ_f) as high as 4.85 GPa [5], but the poor GFA and low plasticity may restrain it as a structure material. It was reported that rare-earth (RE) elements can effectively increase the thermal stability of supercooled liquid and GFA of some Fe-based BMGs [6,7]. Furthermore, the species and concentrations of doped rare earth elements in FeNbB can tune the Curie temperature (T_C) and magnetic performances like magnetocaloric effect (MCE) easily [8–10]. Generally, MCE materials exhibit the maximum isothermal magnetic entropy change ($|\Delta S_M|$) near T_C , which is owing to the transition from ferromagnetic to paramagnetic state, so the value of T_C is a vital parameter in optimization of MCE materials [11,12]. It has been reported by J. Li et al. that (Fe_{0.71}RE_{0.05}B_{0.24})₉₆Nb₄ (RE = Tm, Tb, Ho, Dy) BMGs had large GFA, but their T_C was much higher than room temperature (over 450 K) [8,9]. In order to further adjust the composition to decrease the T_C to

near room temperature, they substituted Fe by Tm with 17 at.% in (Fe_{0.59}Tm_{0.17}B_{0.24})₉₆Nb₄. As a result, the T_C was effectively decreased to 316 K [9]. However, the critical diameter of the glassy alloys is less than 0.5 mm and the cost raises largely [9]. In recent report, Fe₈₇Zr₇B₄Co₂ metallic glass alloy which exhibits a rather high $|\Delta S_M^{pk}|$ near room temperature is regarded as an excellent and promising Fe-rich based MCE material [13]. Nevertheless, it has so poor GFA that only ribbon sample can be prepared. Hence, there is considerable interest in designing Fe-based BMGs with good GFA and T_C near room temperature.

Therefore, in order to fabricate Fe-based BMGs with good GFA and tunable T_C near room temperature, the element Er which is anti-ferromagnetic coupling with Fe [14] was introduced in FeNbB BMG in this work. It is found that the Fe₆₆Er₅Nb₆B₂₃ BMG possesses a critical diameter of 4 mm and a large supercooled liquid region (SCLR) of 90 K. The Fe_{71-x}Er_xNb₆B₂₃ (x = 0, 1, 3, 5, 7 at.%) exhibit T_C of 340–550 K, ΔS_M of 0.74–1.41 J/kg K, and refrigerant capacity (RC_{FWHM}) of 56–112 J/kg in external magnetic field of 1.5 T. Besides, this glassy system also exhibits a high σ_f of 3.09–4.65 GPa and a saturation magnetic flux density of 0.43–1.09 T. The good comprehensive properties of FeErNbB alloys make them very promising as functional materials.

* Corresponding author at: School of Materials Science and Engineering, Jiangsu Key Laboratory for Advanced Metallic Materials, Southeast University, Nanjing 211189, China

E-mail address: blshen@seu.edu.cn (B. Shen).

<https://doi.org/10.1016/j.jnoncrysol.2019.03.005>

Received 22 January 2019; Received in revised form 5 March 2019; Accepted 8 March 2019

Available online 15 March 2019

0022-3093/© 2019 Elsevier B.V. All rights reserved.

2. Experimental

Ribbon samples with nominal compositions of $\text{Fe}_{71-x}\text{Er}_x\text{Nb}_6\text{B}_{23}$ ($x = 0, 1, 3, 5, 7$ at.%) were prepared by melt spinning with a wheel speed of 36 m/s. BMG rods with different diameters were produced by the copper mold casting method. The amorphous structure was ascertained by X-ray diffraction (XRD) with Cu K α radiation. Thermal properties were measured by NETZSCH 404 differential scanning calorimetry (DSC) with a constant heating rate of 40 K/min. Saturation magnetization (M_s) of the ribbons were measured by vibrating sample magnetometer (VSM) in the magnetic field up to 800 kA/m. Temperature dependence of magnetization ($M-T$) and the isothermal magnetization ($M-H$) curves of the amorphous ribbons were measured by SQUID magnetometer (MPMS, Quantum Design R). The compressive fracture strength (σ_f) was determined on 1×2 mm glassy rods with a compressive strain rate $5 \times 10^{-4} \text{ s}^{-1}$ by the Instron testing machine at room temperature. Vickers hardness (H_v) was determined by the Vickers micro-hardness tester under a load of 9.8 N.

3. Results and discussion

Fig. 1 illustrates the DSC traces of the $\text{Fe}_{71-x}\text{Er}_x\text{Nb}_6\text{B}_{23}$ ($x = 0, 1, 3, 5, 7$ at.%) glassy ribbons at a heating rate of 0.67 K/s. The ribbons exhibit an observable glass transition event, followed by a SCLR ($\Delta T_x = T_x - T_g$) and crystallization. The temperatures of the glass transition (T_g) and crystallization onset process (T_x) are clearly marked on the DSC trace in Fig. 1. With increasing Er content of $x = 0, 1, 3, 5, 7$ at.%, T_g and T_x increase gradually from 824 to 946 K and 863 to 996 K, respectively. The SCLR is extended as large as 90 K with 5 at.% Er addition.

Rod samples with critical diameter (D_c) up to 4 mm were prepared in present work. The D_c are 1, 1.5, 2.5, 4 and 2 mm for alloys with Er contents of $x = 0, 1, 3, 5, 7$ at.% respectively. To confirm the fully amorphous structure, the XRD patterns of the as-cast alloy rods are shown in Fig. 2. They all exhibit typical broad humps between 40° and 50° without any crystalline peak on each pattern. It is noteworthy that the peak position (2θ) of the principal diffraction hump is gradually reduced with increasing Er content, which is reasonable as the radius of Er (0.176 nm) is much larger than that of Fe atom (0.126 nm) [15].

Table 1 summarizes the maximum diameter, thermal stability and magnetic properties of the $\text{Fe}_{71-x}\text{Er}_x\text{Nb}_6\text{B}_{23}$ ($x = 0, 1, 3, 5, 7$ at.%) glassy alloys. It can be seen from Table 1 that the alloy system also possesses good soft magnetic performances, including high saturation magnetic flux density (B_s) and low coercivity (H_c) as shown in Fig. 3. The magnetization and H_c for the ribbons are in the range of 1.09 to 0.43 T and 3.42–8.78 A/m, respectively. Due to the coupling of the electron in 3d shell of Fe atom antiferromagnetically with electrons in 4f shell of Er atom, the B_s decreases with the substitution of Fe with Er

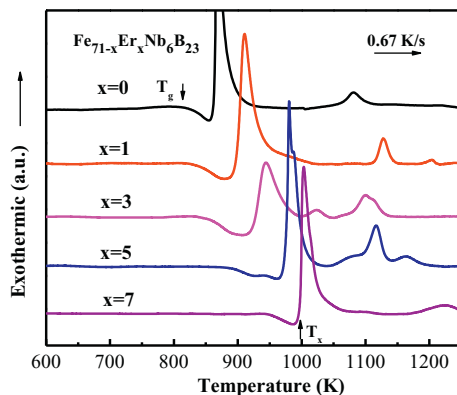


Fig. 1. DSC curves of the melt-spun $\text{Fe}_{71-x}\text{Er}_x\text{Nb}_6\text{B}_{23}$ ($x = 0, 1, 3, 5, 7$ at.%) glassy ribbons.

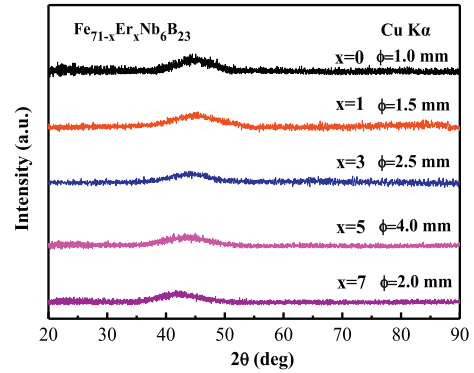


Fig. 2. XRD patterns of the $\text{Fe}_{71-x}\text{Er}_x\text{Nb}_6\text{B}_{23}$ ($x = 0, 1, 3, 5, 7$ at.%) glassy rods with critical diameters of 1, 1.5, 2.5, 4 and 2 mm, respectively.

Table 1

D_c , T_g , T_x , ΔT_x , B_s , H_c of $\text{Fe}_{71-x}\text{Er}_x\text{Nb}_6\text{B}_{23}$ metallic glasses.

Alloys	D_c ϕ (mm)	Thermal stability			Magnetic properties	
		T_g (K)	T_x (K)	ΔT_x (K)	B_s (T)	H_c (A/m)
$\text{Fe}_{71}\text{Er}_0\text{Nb}_6\text{B}_{23}$	1	825	865	40	1.09	3.39
$\text{Fe}_{70}\text{Er}_1\text{Nb}_6\text{B}_{23}$	1.5	827	872	45	1.01	5.34
$\text{Fe}_{68}\text{Er}_3\text{Nb}_6\text{B}_{23}$	2.5	853	920	67	0.71	6.12
$\text{Fe}_{66}\text{Er}_5\text{Nb}_6\text{B}_{23}$	4	882	972	90	0.54	8.78
$\text{Fe}_{65}\text{Er}_7\text{Nb}_6\text{B}_{23}$	2	946	996	50	0.43	5.81

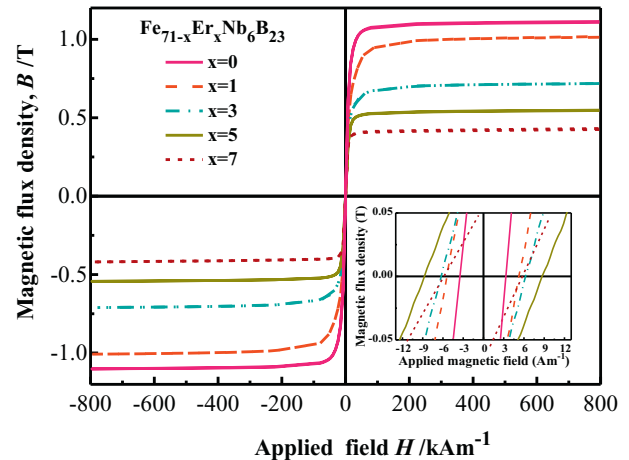


Fig. 3. $B-H$ hysteresis curves of the annealed melt-spun $\text{Fe}_{71-x}\text{Er}_x\text{Nb}_6\text{B}_{23}$ ($x = 0, 1, 3, 5, 7$ at.%) glassy ribbons measured by VSM. The insert is the enlarged $B-H$ loop tracer.

[7]. The H_c increases as the Er content rises to 5 at.% and then decreases with further addition of Er to 7 at.%.

To determine T_c and understand the magnetic properties at high temperatures, thermomagnetic measurements were performed on $\text{Fe}_{71-x}\text{Er}_x\text{Nb}_6\text{B}_{23}$ ($x = 0, 1, 3, 5, 7$ at.%) glassy ribbons. The magnetizations as a function of temperature measured in external magnetic field of 0.02 T are shown in Fig. 4. The inset shows the derivative of the magnetizations (dM/dT) versus temperature. The value of T_c obtained from the minimum of dM/dT varies from 550 K to 340 K for 0–7 at.% Er-containing alloys. The downtrend may be attributed to the antiferromagnetic coupling between Fe and newly introduced Er element [16]. Besides, there are insignificant exchange interactions between the RE and Nb elements [17], therefore doping Er into FeNbB alloy system merely reduces the exchange interactions among Fe atoms. The downtrend of T_c resulted from the increasing content of Er in FeNbB alloy system implies that the room-temperature T_c can effectively

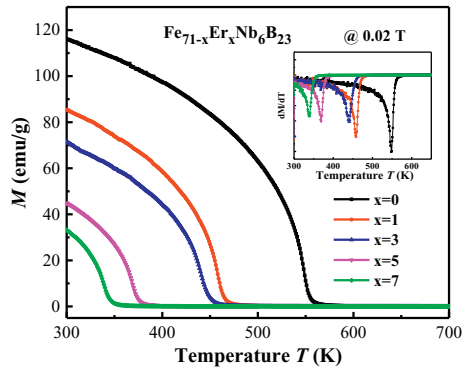


Fig. 4. Temperature dependence of the magnetization and dM/dT versus temperature curves for $\text{Fe}_{71-x}\text{Er}_x\text{Nb}_6\text{B}_{23}$ ($x = 0, 1, 3, 5, 7$ at.%) glassy ribbons under 0.02 T.

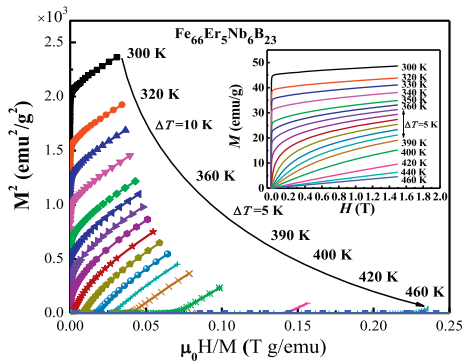


Fig. 5. Arrott plots of $\text{Fe}_{66}\text{Er}_5\text{Nb}_6\text{B}_{23}$ and $\text{Fe}_{71}\text{Nb}_6\text{B}_{23}$ glassy ribbons built from $M(H)$ data. The inset shows the magnetization isotherms of $\text{Fe}_{66}\text{Er}_5\text{Nb}_6\text{B}_{23}$ glassy ribbon measured at temperatures between 300 and 460 K.

realize when doping proper Er content. Based on our results, the T_C of $\text{Fe}_{64}\text{Er}_7\text{Nb}_6\text{B}_{23}$ BMG is about 340 K indicating that this MCE material can be employed near room temperature.

Fig. 5 shows the Arrott plots between 300 K and 460 K, which are calculated from the isothermal $M-H$ curves shown in the inset of Fig. 5. Below T_C , the magnetization saturates rapidly and hardly varies with the external magnetic field after saturation, which shows obvious ferromagnetic character. Above T_C , the magnetization can be regarded as a linear function of the external magnetic field showing the characteristics of paramagnetism. Based on theory of Banerjee criterion [18], if the slope of Arrott plot is negative, the magnetic transition can be viewed as first-order; otherwise, it is second-order magnetic phase transition (SOPT). It can be seen from Fig. 5, all slopes are positive and there is no inflection point, which indicates this alloy system goes through a second-order phase transition. This behavior indicates that the magnetic hysteresis can be reduced, which provides favorable conditions for the application of magnetic refrigeration.

For evaluating the MCE of the BMGs, one of the effective ways is to calculate $|\Delta S_M|$. In the process of isothermal magnetization, the ΔS_M induced by a magnetic field is calculated by a numerically summation of the Maxwell Eq. [19]:

$$|\Delta S_M| = \sum_i \frac{M_i - M_{i+1}}{T_i - T_{i+1}} \Delta H_i \quad (1)$$

where M_i and M_{i+1} are magnetization values measured at temperature T_i and T_{i+1} in a magnetic field H_i , respectively. The temperature dependence of $|\Delta S_M|$ for $\text{Fe}_{71-x}\text{Er}_x\text{Nb}_6\text{B}_{23}$ ($x = 0, 1, 3, 5, 7$ at.%) ribbons in external magnetic field of 1.5 T are shown in Fig. 6. All the samples exhibit a λ -shape curve around T_C , the peak temperature (T_{pk}) of $|\Delta S_M^{pk}|$ shifts to room temperature with the increase of the Er content

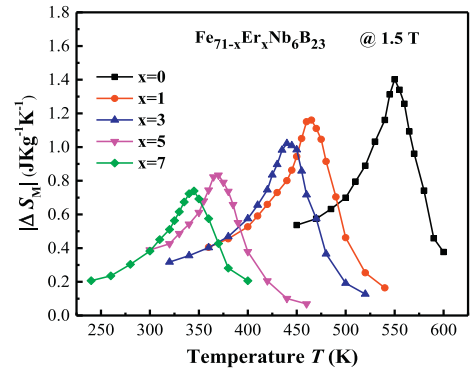


Fig. 6. Temperature dependence of magnetic entropy change of the melt-spun $\text{Fe}_{71-x}\text{Er}_x\text{Nb}_6\text{B}_{23}$ ($x = 0, 1, 3, 5, 7$ at.%) glassy ribbons under a field change of 1.5 T.

from 0 to 7 at.%. Although doping Er in FeNbB alloys results a negative impact on $|\Delta S_M^{pk}|$, which decreases from 1.41 to 0.74 J/kg K, these values are still comparable with other Fe-based metallic glasses [20,21].

To compare the MCE of different materials, the refrigerant capacity has to be considered, which can be expressed as [22,23]:

$$RC_{FWHM} = -\Delta S_M^{pk} \times \delta T_{FWHM} \quad (2)$$

where δT_{FWHM} is the full width at half maximum of the $|\Delta S_M|$ curve. The relationships between applied fields H and $|\Delta S_M|$, RC_{FWHM} for this alloy system are shown in Fig. 7. Both $|\Delta S_M|$ and RC_{FWHM} increase continuously with the improved intensity of magnetic field. The present results of $|\Delta S_M|$ and RC_{FWHM} in external magnetic field of 1.5 T are shown in Table II. For materials with a SOPT, they usually have a positive relation with the applied magnetic fields, the field dependence of both $|\Delta S_M|$ and RC_{FWHM} can be controlled by a power law of the magnetic field [24]:

$$|\Delta S_M^{pk}| \propto H^n \quad (3)$$

$$RC_{FWHM} \propto H^p \quad (4)$$

The values of “ n ” and “ p ” parameters and correlation coefficients are calculated by fitting the experimental results. The experimental and fitted data of $|\Delta S_M|$, RC_{FWHM} using the Eqs. (3) and (4) are shown in Fig. 7. The exponents n and p for alloys with $x = 0, 1, 3, 5, 7$ at. % are 0.76, 0.77, 0.77, 0.77, 0.77 and 1.13, 1.13, 1.14, 1.14, 1.15, respectively. They are remarkably close to those of other Fe-based glassy alloys (i.e., $n = 0.75, p = 1.15$ for $T = T_C$) [25]. It can be found that the value of n and p fluctuates very small, indicating almost the same response of external magnetic field. The exponent n is larger than the prediction of mean field theory (2/3) [26], implying the heterogeneities

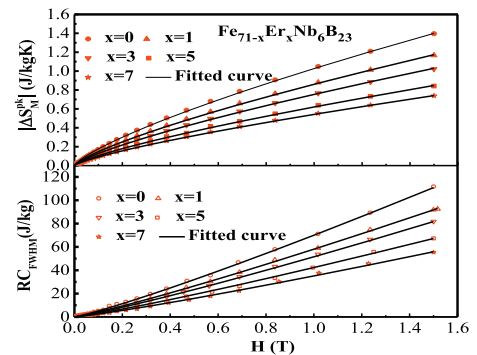


Fig. 7. Extrapolation of the fitted data from 0 to 1.5 T for melt-spun $\text{Fe}_{71-x}\text{Er}_x\text{Nb}_6\text{B}_{23}$ ($x = 0, 1, 3, 5, 7$ at.%) glassy ribbons according to the expression $\Delta S_M \propto H^n$ and $RC_{FWHM} \propto H^p$.

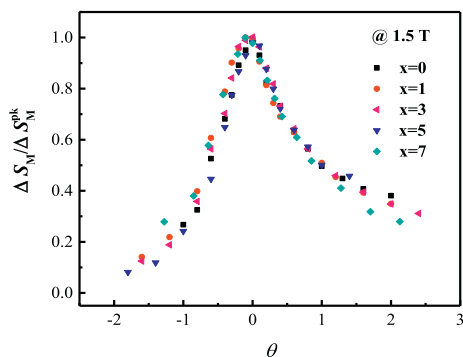


Fig. 8. Universal curves of each $\text{Fe}_{71-x}\text{Er}_x\text{Nb}_6\text{B}_{23}$ ($x = 0, 1, 3, 5, 7$ at.%) glassy alloys as a function of the rescaled temperature θ .

Table 2

T_c , T_{pk} , ΔS_M , RC_{FWHM} , σ_f , H_v of $\text{Fe}_{71-x}\text{Er}_x\text{Nb}_6\text{B}_{23}$ metallic glasses.

Alloys	Magnetocaloric properties				Mechanical properties	
	T_c (K)	T_{pk} (K)	ΔS_M ($\text{Jkg}^{-1}\text{K}^{-1}$)	RC_{FWHM} (Jkg^{-1})	σ_f (GPa)	H_v (kg/mm^2)
$\text{Fe}_{71}\text{Er}_0\text{Nb}_6\text{B}_{23}$	550	550	1.41	112	4.65	1090
$\text{Fe}_{70}\text{Er}_1\text{Nb}_6\text{B}_{23}$	458	463	1.16	92	4.61	1075
$\text{Fe}_{68}\text{Er}_3\text{Nb}_6\text{B}_{23}$	440	444	1.02	82	4.11	1065
$\text{Fe}_{66}\text{Er}_5\text{Nb}_6\text{B}_{23}$	370	370	0.85	67	3.32	1040
$\text{Fe}_{65}\text{Er}_7\text{Nb}_6\text{B}_{23}$	340	345	0.74	56	3.09	1030

exist in this Fe-based alloy system.

As a second-ordered MCE material of FeErNbB, the universal behavior of normalized $\Delta S' = |\Delta S_M|/|\Delta S_M^{pk}|$ can be as a function of θ , which is defined as [27,28]:

$$\theta = \begin{cases} -(T-T_c)/(T_{r1}-T_c), & T \leq T_c \\ (T-T_c)/(T_r2-T_c), & T > T_c \end{cases} \quad (5)$$

T_{r1} and T_{r2} correspond to the temperatures of $0.5 \times |\Delta S_M^{pk}|$. Although the $|\Delta S_M|$ of $\text{Fe}_{71-x}\text{Er}_x\text{Nb}_6\text{B}_{23}$ ($x = 0, 1, 3, 5, 7$ at.%) is different, $\Delta S'(\theta)$ curves are almost overlapped with each other, as shown in Fig. 8. This approximately the same universal behavior of FeErNbB may be related to similar values of exponent n [29]. $\Delta S'(\theta)$ further confirm that this alloy system is a second-order magnetic phase transition system and in accordance with the discussion above.

On the other hand, $\text{Fe}_{71-x}\text{Er}_x\text{Nb}_6\text{B}_{23}$ ($x = 0, 1, 3, 5, 7$ at.%) BMGs also exhibit high σ_f and Vickers hardness, which are also summarized in Table 2. For the Er-containing BMGs, the extremely low ductility and toughness usually lead to premature fracture before reaching their intrinsic material strength [30]. Therefore, to control the deterioration of mechanical properties, the amount of Er element added should be restricted in a proper range.

4. Conclusions

The influences of Er addition on the GFA, magnetic properties and MCE of $\text{Fe}_{71-x}\text{Er}_x\text{Nb}_6\text{B}_{23}$ ($x = 0, 1, 3, 5, 7$ at.%) metallic glasses were studied. The results can be summed up as below:

- (1) The introduction of Er in $\text{Fe}_{71}\text{Nb}_6\text{B}_{23}$ glassy alloy effectively improves the GFA. With 5 at.% Er doping in FeNbB, BMG with diameter of 4 mm was prepared.
- (2) The T_c was modulated by changing the Er concentration from 550 K to 340 K. The $|\Delta S_M|$ and RC_{FWHM} for $\text{Fe}_{71-x}\text{Er}_x\text{Nb}_6\text{B}_{23}$ ($x = 0, 1, 3, 5, 7$ at.%) ribbons decrease with an increase of Er content. Under a field of 1.5 T, the maximum $|\Delta S_M|$ for $\text{Fe}_{71-x}\text{Er}_x\text{Nb}_6\text{B}_{23}$ ($x = 0, 1, 3,$

5, 7 at.%) are 1.41, 1.16, 1.02, 0.85, 0.74 $\text{Jkg}^{-1}\text{K}^{-1}$, respectively. The RC_{FWHM} are 112, 92, 82, 67 and 56 J/kg for $x = 0, 1, 3, 5, 7$, respectively.

- (3) These BMGs also exhibit high B_s of 1.09–0.43 T, strong σ_f of 4.65–3.09 GPa and large Vickers hardness of 1090–1030 kg/mm^2 , respectively. These excellent properties make the Fe-based ferromagnetic BMGs promising as structural materials for future applications.

Acknowledgement

This work was supported by the National Natural Science Foundation of China (Grant Nos. 51631003, 51471050, 51601130), the State Key Development Program for Basic Research of China (Grant No. 2016YFB0300502), Jiangsu Key Laboratory for Advanced Metallic Materials (Grant No. BM2007204), the Fundamental Research Funds for the Central Universities (Grant No. 2242017 K40189).

Declaration of interest statement

The authors declared that they have no conflicts of interest to this work. We declare that we do not have any commercial or associative interest that represents a conflict of interest in connection with the work submitted.

References

- [1] W.M. Yang, H.S. Liu, Y.C. Zhao, A. Inoue, K. Jiang, J.T. Huo, H.B. Ling, Q. Li, B.L. Shen, Mechanical properties and structural features of novel Fe-based bulk metallic glasses with unprecedented plasticity, *Sci. Rep.* 4 (2014) 6233.
- [2] A.D. Wang, M.X. Zhang, J.H. Zhang, H. Men, B.L. Shen, S.J. Pang, T. Zhang, FeNiPBn bulk glassy alloys with good soft-magnetic properties, *J. Alloys Compd.* 536 (2012) S354–S358.
- [3] W.H. Wang, C. Dong, C.H. Shek, Bulk metallic glasses, *Mater. Sci. Eng. R* 44 (2004) 45–89.
- [4] J.E. Gao, Z.P. Chen, Q. Du, H.X. Li, Y. Wu, H. Wang, X.J. Liu, Z.P. Lu, Fe-based bulk metallic glass composites without any metalloids elements, *Acta Mater.* 61 (2013) 3214–3223.
- [5] J.H. Yao, J.Q. Wang, Y. Li, Ductile Fe-Nb-B bulk metallic glass with ultrahigh strength, *Appl. Phys. Lett.* 92 (2008) 251906.
- [6] D.H. Kim, J.M. Park, D.H. Kim, W.T. Kim, Development of quaternary Fe-B-Y-Nb bulk glassy alloys with high glass-forming ability, *J. Mater. Res.* 22 (2007) 471–477.
- [7] J.W. Li, A.N. He, B.L. Shen, Effect of Tb addition on the thermal stability, glass-forming ability and magnetic properties of Fe-B-Si-Nb bulk metallic glass, *J. Alloys Compd.* 586 (2014) S46–S49.
- [8] J.W. Li, J.Y. Law, J.T. Huo, A.N. He, Q.K. Man, C.T. Chang, H. Men, J.Q. Wang, X.M. Wang, R.W. Li, Magnetocaloric effect of Fe-RE-B-Nb (RE = Tb, Ho or Tm) bulk metallic glasses with high glass-forming ability, *J. Alloys Compd.* 644 (2015) 346–349.
- [9] J.W. Li, J.Y. Law, H.M. Ma, A.N. He, Q.K. Man, H. Men, J.T. Huo, C.T. Chang, X.M. Wang, R.W. Li, Magnetocaloric effect in Fe-Tm-B-Nb metallic glasses near room temperature, *J. Non-Cryst. Solids* 425 (2015) 114–117.
- [10] J.W. Li, J.T. Huo, J.Y. Law, C.T. Chang, J. Du, Q.K. Man, X.M. Wang, R.W. Li, Magnetocaloric effect in heavy rare-earth elements doped Fe-based bulk metallic glasses with tunable curie temperature, *J. Appl. Phys.* (6) (2014) 063902.
- [11] F.X. Hu, B.G. Shen, J.R. Sun, Magnetic entropy change in $\text{Ni}_{51.5}\text{Mn}_{22.7}\text{Ga}_{25.8}$ alloy, *Appl. Phys. Lett.* 76 (2000) 3460–3462.
- [12] O. Tegus, E. Bruck, K.H.J. Buschow, F.R. de Boer, Transition-metal-based magnetic refrigerants for room-temperature applications, *Nature* 415 (2002) 150–152.
- [13] P. Yu, J.Z. Zhang, L. Xia, $\text{Fe}_{87}\text{Zr}_7\text{B}_4\text{Co}_2$ amorphous alloy with excellent magnetocaloric effect near room temperature, *Intermetallics* 95 (2018) 85–88.
- [14] K.H.J. Buschow, Intermetallic compounds of rare-earth and 3d transition metals, *Rep. Prog. Phys.* 40 (1977) 1179.
- [15] J.G. Speight, *Lang's Handbook of Chemistry*, 16th ed., Mc Graw-Hill, London, 2005, p. 1.151.
- [16] S. Legvold, E.P. Wohlfarth (Ed.), *Handbook of Magnetic Materials*, vol. 1, North-Holland, Amsterdam, 1980, p. 189.
- [17] A. Chrobak, V. Nosenko, G. Hanecek, L. Boichyshyn, B. Kotur, A. Bajorek, O. Zivotsky, A. Hendrych, Effect of rare earth additions on magnetic properties of $\text{Fe}_{82}\text{Nb}_2\text{B}_{14}\text{RE}_2$ (RE = Y, Gd, Tb and Dy) amorphous alloys, *Mater. Chem. Phys.* 130 (2011) 603.
- [18] S.K. Banerjee, On a generalised approach to first and second order magnetic transitions, *Appl. Phys. Lett.* 12 (1964) 16–17.
- [19] R.D. McMichael, J.J. Ritter, R.D. Shull, Enhanced magnetocaloric effect in $\text{Gd}_3\text{Ga}_5-x\text{Fe}_x\text{O}_{12}$, *J. Appl. Phys.* 73 (1993) 736946.
- [20] K. Sarlar, E. Civan, I. Kucuk, Magnetocaloric effect and temperature-dependent

- magnetoresistance in Cu-doped FeCoNiBSiNb amorphous alloys, *J. Non-Cryst. Solids* 471 (2017) 169–174.
- [21] H.Y. Zhang, R. Li, T. Xu, F.M. Liu, T. Zhang, Near room-temperature magnetocaloric effect in FeMnPBC metallic glasses with tunable Curie temperature, *J. Magn. Magn. Mater.* 347 (2013) 131–135.
- [22] K.A. Jr. Gschneidner, V.K. Pecharsky, Magnetocaloric materials, *Annu. Rev. Mater. Sci.* 30 (2000) 387–429.
- [23] J.Y. Law, R.V. Ramanujan, V. Franco, Tunable Curie temperatures in Gd alloyed Fe-B-Cr magnetocaloric materials, *J. Alloys Compd.* 508 (2010) 14–19.
- [24] V. Franco, A. Conde, Scaling laws for the magnetocaloric effect in second order phase transitions: from physics to applications for the characterization of materials, *Int. J. Refrig.* 33 (2010) 465–473.
- [25] V. Franco, J.S. Blazquez, B. Ingale, A. Conde, The magnetocaloric effect and magnetic refrigeration near room temperature: materials and models, in: D.R. Clarke (Ed.), *Annual Review of Materials Research*, vol. 42, 2012, pp. 305–342.
- [26] H. Oesterreicher, F.T. Parker, Magnetic cooling near Curie temperatures above 300 K, *J. Appl. Phys.* 55 (1984) 4334–4338.
- [27] V. Franco, J.S. Blazquez, A. Conde, Field dependence of the magnetocaloric effect in materials with a second order phase transition: a master curve for the magnetic entropy change, *Appl. Phys. Lett.* 89 (2006) 222512.
- [28] V. Franco, A. Conde, J.M. Romero-Enrique, J.S. Blazquez, An universal curve for the magnetocaloric effect: an analysis based on scaling relations, *J. Phys. Condens. Matter* 20 (2008) 285207.
- [29] H.Y. Zhang, J.T. Ouyang, D. Ding, H.L. Li, J.G. Wang, W.H. Li, Influence of Fe substitution on thermal stability and magnetocaloric effect of Gd₆₀Co_{40-x}Fe_x amorphous alloy, *J. Alloys Compd.* 769 (2018) 186–192.
- [30] Z.Q. Liu, Z.F. Zhang, Mechanical properties of structural amorphous steels: intrinsic correlations, conflicts, and optimizing strategies, *J. Appl. Phys.* 114 (2013) 243519.